CFSRC COLLOQUIUM

Proceedings of the Cold-Formed Steel Research Consortium Colloquium
20-22 October 2020 (cfsrc.org)

Numerical investigation of the impact of bearing condition on the axial behavior of variable-height cold-formed steel stud wall assemblies

Abbas Joorabchian[1], Zhanjie Li [2], Kara D. Peterman[3]

Abstract

This paper is devoted to identifying and numerically characterizing the strength of cold-formed steel (CFS) wall assemblies of various height with non-uniform bearing conditions. The results are for a means of evaluating existing design guidelines presented in the North American Specification of the American Iron and Steel Institute (AISI S100-16). In this standard, the bearing condition of the members is not included in equations for predicting axial strength. However, based on the recent experiments done by the authors, non-uniform stress distributions at the ends of CFS studs, caused by different bearing conditions, can reduce the axial capacity of the assemblies. The sources of nonuniformity considered were finite flexibility of the concrete slabs, uneven bearing surfaces provided by the slabs, distance of the wall assemblies to the slab edge, or overhang conditions caused by construction error. In the experiments done by the authors, the height of lipped-channels was fixed to 12 inches to enable comparison across specimens. However, in typical construction, wall assemblies installed on concrete slabs are generally full-height (8 ft or higher) and thus globally-dominant. In this paper, various heights are considered for the studs. They are determined based on the local, distortional, and global buckling half-wavelengths. The impact of bearing conditions on the strength is further elucidated via high-fidelity 3D finite element analyses (FEA). The results of FEAs clarify how the non-uniform stress distribution at the ends of the studs or partial bearing conditions can impact their strengths when they buckle locally, distortionally, and globally. The finite element models are calibrated with existing experimental results. Comparison to available experimental results and to the governing design codes are provided.

1. Introduction

Cold-formed steel (CFS) wall assemblies are constructed by a system of repetitive vertical studs which are capped between horizontal tracks at the top and bottom. Studs are typically spaced 12, 16, or 24 inches (30.48, 35.56, or 40.64 cm) apart. These wall assemblies can be interior or exterior load-bearing walls that are typically placed on concrete slab floors of modern structures. These compression members can have variable heights from short ones which are used under the openings of the walls to full scale members (~ 8 ft [2.44 m] in height). Stability behavior of CFS studs is dependent on member height. They can buckle locally, distortional, globally, or a combination of these buckling modes. Complicating this, exterior CFS wall assemblies are placed close to or at the edge of concrete slabs creating a non-uniform bearing condition at the stud ends. Due to construction errors, some of the studs overhang from slab edges and have a partial bearing condition at their ends since a part of the assembly is placed outside of the concrete slab. These phenomena lead to a reduction in axial capacity of CFS wall assemblies, which is especially true for short, locally and distortionally dominant members. The design guidelines for calculating axial capacity of members in the North American Specification of the American Iron and Steel Institute (AISI S100-16) [1] does not consider the impact of bearing conditions on the behavior of members and assumes a uniform stress distribution at their ends.

In most of the recent research projects on the behavior of CFS members under the compression, concrete slabs are ignored [2–7]. In the experimental projects, the assemblies either were mounted on a rigid support, such as a rigid steel plate or beam, or on the laboratory floor. Bae, et al [8] and

[1] Graduate Research Assistant, Department of Civil & Environmental Engineering, University of Massachusetts Amherst, ajoorabchian@umass.edu
[2] Assistant Professor, Department of Engineering, The SUNY Polytechnic Institute, zhanjie.li@sunypoly.edu
[3] Assistant Professor, Department of Civil & Environmental Engineering, University of Massachusetts Amherst, kdpeterman@umass.edu

Polyzois and Fox [9] included concrete slabs in their experiments to investigate the impact of non-uniform bearing condition on the behavior of CFS assemblies. Both of the researchs concluded that edge distances impact the system strength. While these studies emphasize on the critical role of concret slabs and bearing conditions, they were limited to one stud-track size. Moreover, they just considered a few edge distances – mainly far from the edge – and did not examine intermediate distances. To fill these gaps, a series of experiments and numerical analysis were conduted by the authors [10–13]. A variety of stud-track assemblies with a wide range of edge distances, including overhang bearing conditions, on concrete slabs were explored. It was concluded that by moving the assemblies close to the edge, the strength was decreased by 6%-24% for at edge bearing condition. This reduction was more significant in overhang conditions and was 12%-40%. The results revealed that the impact of bearing conditions should be considered in design specifications for measuring the compressive strength of members. However, the length of studs in this research, which was the first phase of a comprehensive research project, was fixed to 12 inches (30.48 cm) resulting in buckling failure modes that were a combination of local and distortional buckling [10–13].

The second phase of the research project characterizes, experimentally and computationally, the relation between bearing conditions and compressive strength of CFS wall assemblies specifically examining the impact to each buckling mode (local, distortional, and global). In this paper, a part of the computational analysis of this work is presented, elucidating the impact of bearing conditions on local, distortional, and global buckling behaviors.

2. Computational modeling matrix

In this research, studs with 33, 54, and 68 mil (0.84, 1.37, and 1.73 mm) thickness are used. The height and flange length of all the studs were fixed 3.62 and 1.62 inches (91.9 and 41.1 mm), respectively. The thickness of tracks matched to the stud thickness. The height of tracks was 3.62 inches (91.9 mm); their flange width was all fixed 1.25 inches (31.75 mm). Table 1 represents the computational modeling matrix of the project.

Stud heights are determined from their buckling mode half-wave length; thus, the physical heights of each configuration differ for local and distortional modes. Schematics of different bearing conditions are illustrated in Figure 1. In this paper, only the results of assemblies including 362S162-33 and 362S162-68 are presented.

Table 1: Numerical modeling matrix.

Stud	Track	Stud height	Bearing condition
362S162-33	362T125-33	Local Distortional 96"	Full bearing, at the edge, 1" (25.4 mm) Overhang
362S162-54	362T125-54	Local Distortional 96"	Full bearing, at the edge, 1" (25.4 mm) Overhang
362S162-68	362T125-68	Local Distortional 96"	Full bearing, at the edge, 1" (25.4 mm) Overhang

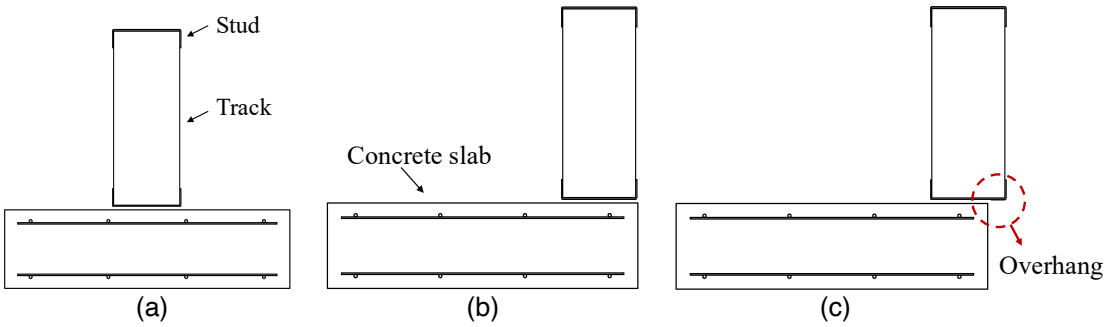

Figure 1: Schematic of bearing conditions; (a) Full bearing condition, (b) at the edge bearing condition, (c) 1 inch (25.4 mm) bearing condition.

Assemblies consists of CFS wall assemblies and concrete slabs. CFS stud-track assemblies include two studs, 12 inches (30.48 cm) apart, and two 24-inches (60.96 cm) tracks at the top and bottom. The dimension of concrete slabs is 22×34×6 inches (55.88×86.36×15.24 cm). Two layers of reinforcement are provided at the top and bottom of concrete slabs [12]. Figure 2 provides a schematic of specimens and dimensions.

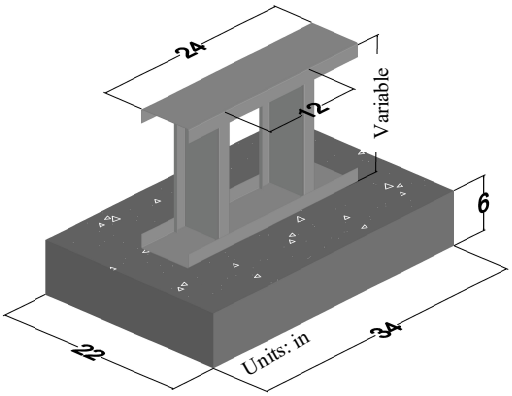

Figure 2: Schematic of specimens and dimensions.

3. Calculating stud height

Stud height is calculated such that the stud is permitted to buckle either locally, distortionally, or globally. Stud height is determined through conducting elastic buckling analysis via finite strip method software CUFSM [14–16]. Figure 3 illustrates signature curve of 362S162-68.

The lengths at which the local and distortional buckling occur are the corresponding half-wave lengths of first and second minima, respectively. For the global buckling, the length equal to 8 ft (2.44 m) is considered for both of the sections. The lengths are summarized in Table 2.

Table 2: Determined height of studs for different buckling modes.

Stud	**Length** *in (cm)*		
	Local	Distortional	Global
362S162-33	2.85 (7.24)	17.48 (44.40)	96 (243.84)
362S162-68	2.90 (7.37)	11.50 (29.21)	96 (243.84)

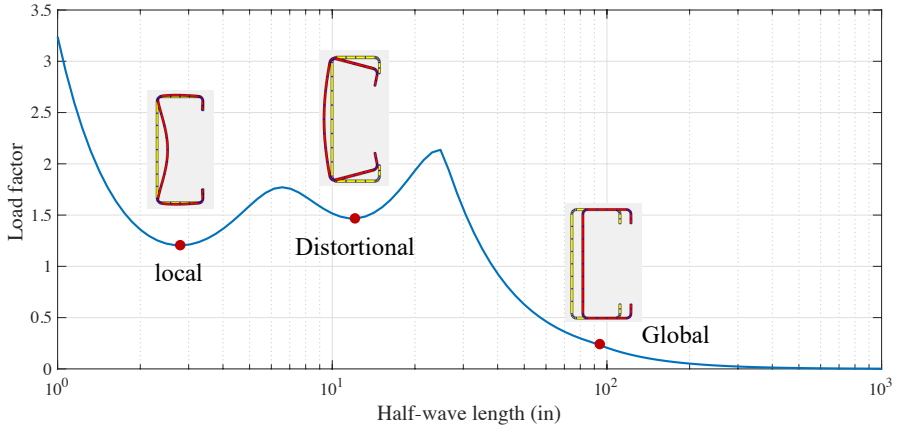

Figure 3: Signature curve of 362S162-68.

4. High-fidelity finite element modeling

ABAQUS [17], a commercial finite element software, is used for high-fidelity non-linear analysis. Nominal dimensions are used for simulating the members. CFS members are modeled using 4-node shell element (S4R). For concrete slabs, 8-node hexahedral elements (C3D8R) are utilized. Reinforcements are modeled by two-node three-dimensional truss elements at two layers at the top and bottom of concrete slabs [13].

Stress-strain relation of CFS members was measured directly in the laboratory [12]. For 68 mil (1.73 mm) specimens, stress-strain curve of 54 mil specimens presented in [12] is utilized. In order to modeling in ABAQUS, engineering stress-strain relations are converted to true stress-strain curve using Eqs. (1) and (2). Measured modulus of elasticity was defined for CFS materials, and Poisson's ratio was considered as 0.3.

$$\sigma_{true} = \sigma_{eng}(1+\varepsilon_{eng}) \quad (1)$$

$$\varepsilon_{true} = ln(1+\varepsilon_{eng}) \quad (2)$$

Compressive and tensile strength of concrete were measured directly. The compressive strength was 4.8 ksi (33.2 MPa) and the tensile one was 0.3 ksi (2.3 MPa) [12],[13]. Since only two peak strengths are available, the stress-strain behavior of concrete is estimated and generated. The Hognestad parabola is employed to simulate the compressive constitutive relationship of concrete [13],[18]. Uniaxial tensile behavior of concrete is modeled using a linear behavior until the tensile strength and a bilinear one after cracking, as described thoroughly in [13].

In order to simulate the fasteners fastening the studs to tracks, multi-point constraints (MPC pin) are utilized. Steel-to-concrete pins are modeled using MPC pin as well. Interaction between surfaces is simulated by surface-to-surface contact. To simulate the interaction between the stud ends and tracks web, node-to-surface contact is deployed. "Finite sliding" formulation is employed for surface-to-surface interactions, and "small sliding" is used for "node-to-surface" contacts [13]. The normal and tangential behaviors of contacts are modeled using "hard contact" and "frictionless" formulations, respectively. All degrees of freedom (DOF) of all the nodes of bottom of concrete slab are fixed. Moreover, all transitional degrees of freedom, except longitudinal, of the top track nodes are Interaction between surfaces is simulated by surface-to-surface contact. To simulate the interaction between the stud ends and tracks web, node-to-surface contact is deployed. "Finite sliding" formulation is employed for surface-to-surface interactions, and "small sliding" is used for "node-to-surface" contacts [13]. The normal and tangential behaviors of contacts are modeled using "hard contact" and "frictionless" formulations, respectively. All degrees of freedom (DOF) of all the nodes of bottom of concrete slab are fixed. Moreover, all transitional degrees of freedom, except longitudinal, of the top track nodes are restrained. A uniform displacement control load is applied to the top track. A developed finite element model for 68 mil specimen, 11.5 inches (29.21 cm) in height, placed at edge of concrete slab is represented in Figure 4.

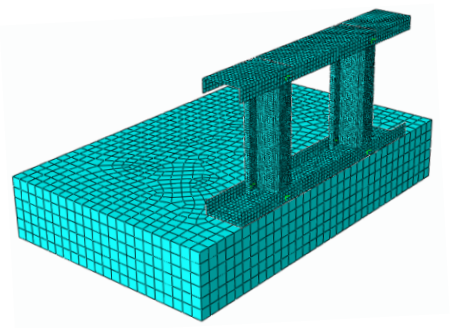

Figure 4: Simulated finite element and mesh discretization of 68 mil assembly fastened at the edge of concrete slab.

More detail about developing the finite element models of CFS wall assemblies and concrete slabs can be found in [13].

5. Finite element results

In total, 24 high-fidelity finite element models, including the assemblies described in Table 1 and assemblies with rigid bearing condition (no concrete slab), are simulated and analyzed. Figure 5 illustrates force-displacement plots and Table 3 and Table 4 show the results for each buckling mode separately. The peak loads of each assembly are compared to the compressive strength of the assembly with rigid bearing condition (P_{max_R}). When the assemblies are placed at the edge, the axial force reduction is between 3%-17%. When the assemblies are placed at the edge, the non-uniform stress distribution at the end of studs affects the axial strength of CFS wall assemblies. The maximum reduction is for local buckling mode, where the assemblies have the highest compressive strength. However, in the full-scale specimens in which global buckling is dominant, the impact of concrete slab and non-uniform bearing condition is minimized due to the fact that in this buckling mode, the strength of CFS assembly is decreased significantly and the

studs buckle before distribution of load into the slab. However, in the local and distortional buckling modes, due to the higher axial capacity, the force is distributed into the concrete prior to failure.

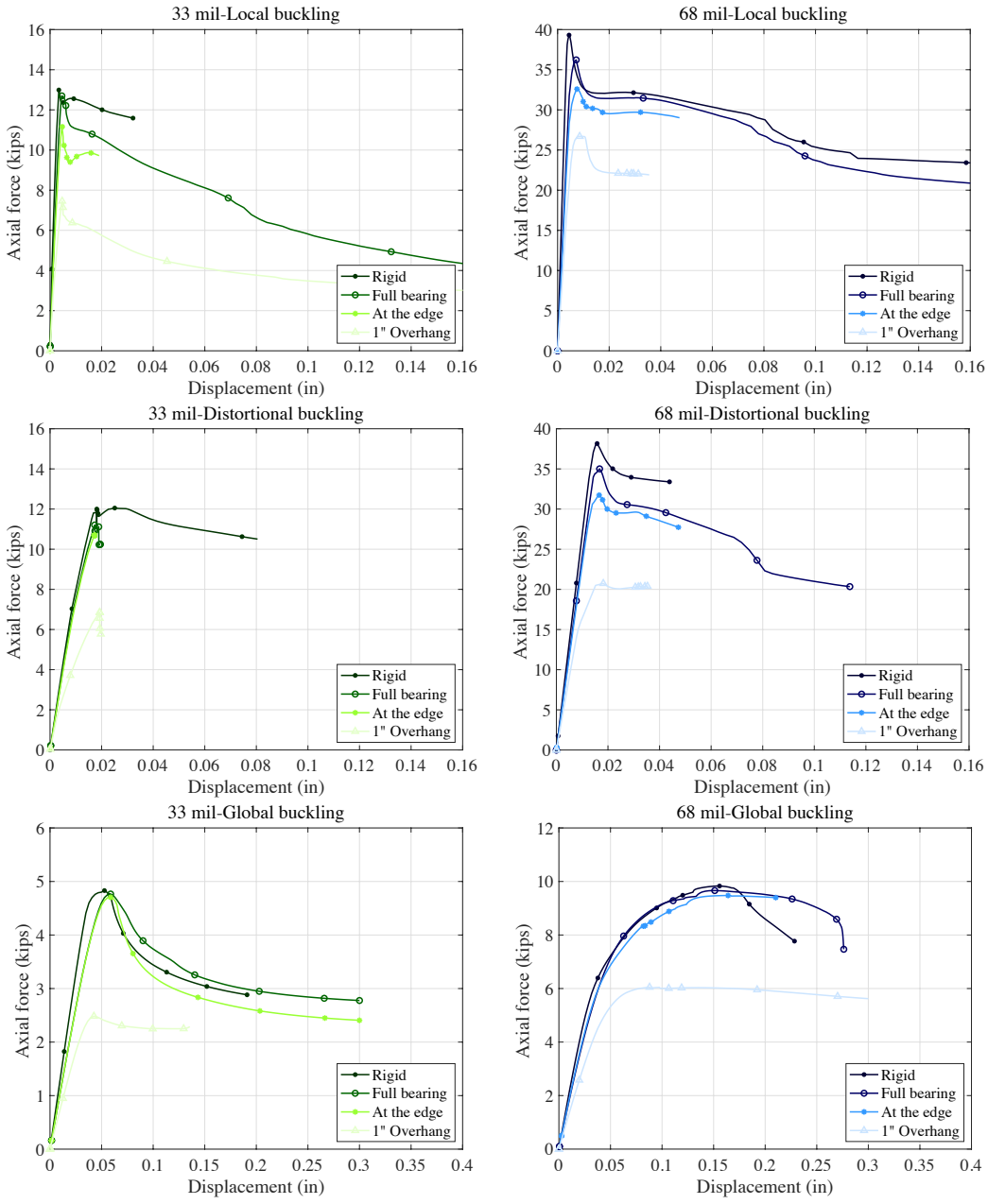

Figure 5: Force-displacement of curves of finite element analyses.

In overhang bearing conditions, the reduction is between 32%-48%. In these conditions the reduction in strength is magnified due to two factors: non-uniform stress distribution, and partial bearing conditions that lead to a potential load

eccentricity, which compound in their impact on axial capacity.

6. Comparing finite element results with AISI S100-16 prediction methods

In order to validate finite element results and examining the impact of non-uniform bearing condition on the proposed methods by AISI S100-16 specification for calculating compressive strength of members, the capacity of each assembly is calculated according to AISI S100-16. For rigid, full, and at the bearing conditions, equations given for members in compression (chapter E) are utilized. Since there is an eccentricity and a bending moment in the assemblies overhanging from slab, the method proposed in chapter H for members under combined axial load and bending is used. Calculated eccentricities for 33 mil and 68 mil (0.84 mm and 1.73 mm) assemblies are 0.084 and 0.089 in. (2.13 and 2.26 mm), respectively. The results of comparison are summarized in Table 3 and Table 4.

Table 3: Summary of finite element analysis results and AISI S100-16 predicted capacities for 33 mil (0.84 mm) assemblies.

Stud section	Bearing condition	Buckling mode	FEM (P_{max})	1- (P_{max}/P_{max_R})	AISI S100-16		P_{max}/P_n
					P_n	ϕP_n	
			kips (kN)	*%*	*kips (kN)*	*kips (kN)*	*kips/kips*
362S162-33	Local	Rigid	12.7 (56.4)	—	13.35 (59.4)	11.3 (50.5)	0.95
		Full	12.6 (55.9)	1	13.35 (59.4)	11.3 (50.5)	0.94
		Edge	11.2 (49.8)	12	13.35 (59.4)	11.3 (50.5)	0.84
		1" Overhang	7.5 (33.4)	41	10.03 (44.6)	8.7 (38.5)	0.75
	Distortional	Rigid	12.0 (53.4)	—	12.9 (57.4)	11.0 (48.8)	0.93
		Full	11.2 (49.8)	7	12.9 (57.4)	11.0 (48.8)	0.87
		Edge	10.7 (47.6)	11	12.9 (57.4)	11.0 (48.8)	0.83
		1" Overhang	6.9 (30.7)	43	9.8 (43.5)	8.4 (37.5)	0.71
	Global	Rigid	4.9 (21.5)	—	5.0 (22.1)	5.0 (22.1)	0.98
		Full	4.8 (21.4)	1	5.0 (22.1)	5.0 (22.1)	0.97
		Edge	4.7 (20.9)	3	5.0 (22.1)	5.0 (22.1)	0.95
		1" Overhang	2.5 (11.1)	48	4.4 (19.7)	3.8 (16.8)	0.57

Table 4: Summary of finite element analysis results and AISI S100-16 predicted capacities for 68 mil (1.73 mm) assemblies.

Stud section	Bearing condition	Buckling mode	FEM (P_{max})	1- (P_{max}/P_{max_R})	AISI S100-16		P_{max}/P_n
					P_n	ϕP_n	
			kips (kN)	*%*	*kips (kN)*	*kips (kN)*	*kips/kips*
362S162-68	Local	Rigid	39.3 (174.9)	—	42.3 (188.3)	36.0 (160.1)	0.93
		Full	36.2 (161.1)	8	42.3 (188.3)	36.0 (160.1)	0.86
		Edge	32.6 (145.0)	17	42.3 (188.3)	36.0 (160.1)	0.77
		1" Overhang	26.7 (118.8)	32	33.7 (149.7)	28.9 (128.7)	0.79
	Distortional	Rigid	38.2 (169.7)	—	42.3 (188.3)	36.0 (160.1)	0.90
		Full	35.0 (155.7)	8	42.3 (188.3)	36.0 (160.1)	0.83
		Edge	31.7 (141.1)	17	42.3 (188.3)	36.0 (160.1)	0.75
		1" Overhang	20.7 (92.2)	46	33.7 (149.7)	28.9 (128.7)	0.62
	Global	Rigid	9.8 (43.7)	—	10.2 (45.3)	8.7 (38.5)	0.96
		Full	9.7 (43.0)	2	10.2 (45.3)	8.7 (38.5)	0.95
		Edge	9.5 (42.1)	4	10.2 (45.3)	8.7 (38.5)	0.93
		1" Overhang	6.0 (26.8)	39	9.6 (42.6)	8.2 (36.4)	0.63

While the prediction of AISI S100-16 for assemblies buckling either locally or distortionally is accurate in full bearing conditions, it is poor when they are placed at the edge. This proves when there is enough distance between CFS assemblies and the slab edge, concrete slab can maintain a uniform stress distribution. However, since the proposed methods in the design specifications are based on the uniform stress-distribution at the ends of the members, they cannot predict the axial capacity accurately. AISI S100-16 predicts well the axial capacities of globally-dominant specimens with not only full bearing but also edge bearing condition. Therefore, when the axial capacity of the members is too low, like global buckling mode, the concrete slab does not impact the axial behavior of CFS wall

assemblies and the AISI S100-16 is able to predict accurately the strength of members even when they are placed at the edge. The impact of bearing condition on the compressive strength of assemblies has a direct relation with strength of assemblies, and for low-strength systems, the impact of concrete slab and bearing condition can be ignored. The predicted capacity for overhang bearing conditions is too poor for all the assemblies, which is due to the impact of placing a part of the system outside of the slab alongside the impact of non-uniform bearing condition. Hence, proposing reduction factors for improving the existing design specifications is needed.

7. Conclusion

The impact of non and partial bearing conditions on the axial behavior of variable-height CFS assemblies was explored computationally. It is concluded when there is enough edge distance, the concrete slab can keep the stress distribution uniform regardless of cross-section and height of members. For the assemblies buckling globally, the impact of edge bearing condition is negligible and proposed methods in AISI S100-16 can accurately predict the strength. In shorter assemblies buckling either locally or distortionally, the edge bearing condition provides a non-uniform stress distribution at the ends of CFS studs, which decreases the axial strength of assemblies 11%-17%, where this reduction is more significant in thicker specimens. In overhang bearing conditions, a part of the CFS assembly is placed outside of the slab, which in addition to the impact of non-uniform bearing condition decrease the strength of assemblies dramatically. The prediction of AISI S100-16 is too poor for all the stud-track assemblies with overhang bearing conditions regardless of their height. Therefore, improvement of current design specifications by defining reduction factors would be beneficial.

8. Future work

In the first phase of this comprehensive research project ([12],[13]), the impact of bearing conditions on the behavior of fixed-height CFS assemblies was studied thoroughly. In the second phase of the project, the experiments of the assemblies discussed herein will be conducted at Gunness and Brack structural laboratory of the University of Massachusetts Amherst. The procedure of the tests would be the same as what is described in [12] and [13]. The schematic of new assemblies with variable height is shown in Figure 6.

Furthermore, in order to extend the utility of the results of first phase to variable-height walls and a range of cross-section, a computational modeling program is defined. In this program, in total, 2376 high-fidelity 3D finite element analyses of variable-height stud assemblies bearing on reinforcement concrete slabs will be performed in ABAQUS. 66 different cross-sections, representing common wall stud members, will be investigated. The position of the wall assemblies on the concrete slab will be varied, from full-b earing condition with no edge effects to intermediate edge distances approaching the edge, to the slab edge itself, and overhanging from the edge.

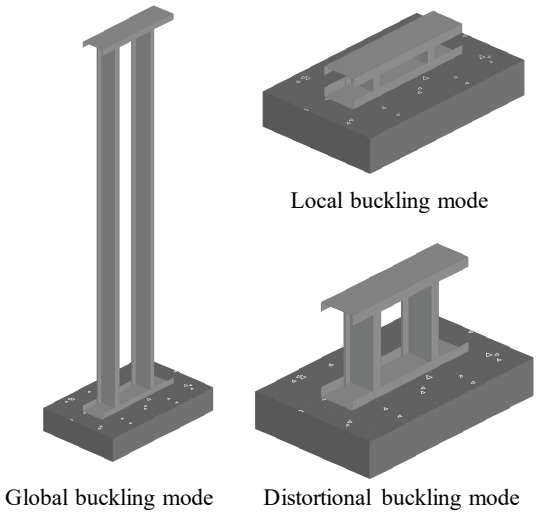

Figure 6: Schematic of the assemblies for the second phase of the research project.

9. Acknowledgement

The authors would like to gratefully thank American Iron and Steel Institute (AISI) for their financial support and Mark Gauthier, the University of Massachusetts Amherst lab technician for his help.

References

[1] AISI S100, North America Specification for the Desighn of Cold-Formed Steel Structures, American Iron and Steel Institude, Washington, D.C., 2016.

[2] T.H. Miller, T. Pekoz, “Behavior of cold-formed steel wall stud assemblies,” Journal of structural engineering, vol. 119, no. 2, pp. 641–651, 1993.

[3] Y. Telue, M. Mahendran, “Behaviour of cold-formed steel wall frames lined with plasterboard,” Journal of Constructional Steel Research, vol. 57, pp. 435–452, 2001.

[4] R.A. Laboube, P.F. Findlay, “Wall Stud-to-Track Gap : Experimental Investigation,” Journal of Architectural Engineering, vol. 13, no. 2, pp. 105–110, 2007.

[5] J. Wang, Y.S. Tian, and T. J. Lu, “The role of frame members and sheathing in partition wall panels subjected to compression,” Journal of thin-walled structures, vol. 43, pp. 983–1002, 2005.

[6] L.C.M. Vieira, Y. Shifferaw, and B. W. Schafer, “Experiments on sheathed cold-formed steel studs in compression,” Journal of Constructional Steel Research, vol. 67, no. 10, pp. 1554–1566, 2011.

[7] K.D. Peterman, B. W. Schafer, “Sheated cold-formed steed studs under axial and lateral load,” Journal of Constructional Steel Research, vol. 140, no. 10, pp. 1–12, 2014.

[8] S. Bae, A. Belarbi, and R. A. LaBoube, “Bearing Strength of Slabs on Grade Supporting a Cold-Formed Steel Wall in Low-Rise Building,” Journal of Architectural Engineering, vol. 12, no. 1, pp. 24–32, 2006.

[9] D. Polyzois, S. Fox, “Bearing of Steel Studs on Concrete,” Newsletter for the Light Gauge Steel Engineering Association (now the Cold-Formed Steel Engineering Institute), 2011.

[10] A. Joorabchian, Z. Li, and K.D. Peterman, “The Impact of Bearing Conditions on the Behavior of Cold- Formed Steel Stud Assemblies,” Proc. of International Specially Conference on Cold-Formed Steel Structures, St. Louis, Missouri, 2018.

[11] A. Joorabchian, Z. Li, and K.D. Peterman, “The Impact of Bearing Conditions on the Stability Behavior of Cold- Formed Steel Stud Assemblies,” Proc. of the Annual Stability Conference, Structural Stability Research Counsile, St. Louis, Missouri-Rolla, 2019.

[12] A. Joorabchian, Z. Li, and K.D. Peterman, “Steel stud assemblies bearing on concrete slabs (Phase 1),” American Iron and Steel Institude (AISI), 2019.

[13] A. Joorabchian, Z. Li, and K.D. Peterman, “Experimental and numerical investigation of fixed-height cold-formed steel wall assemblies bearing on concrete slabs”, Thin-walled Structures, 2020 <submitted>

[14] B.W. Schafer, S. Ádány, “Buckling analysis of cold-formed steel members using CUFSM: conventional and constrained finite strip method,” Proc. of 18th International Specialty Conference on Cold-Formed Steel Structures, Orlando, FL, 2006.

[15] Z. Li, B.W. Schafer, “Buckling analysis of cold-formed steel members with general boundary conditions using CUFSM: conventional and constrained finite strip methods,” Proc. of International Specially Conference on Cold-Formed Steel Structures, St. Louis, Missouri, 2010.

[16] A. Joorabchian, K.D. Peterman, “Using Photogrammetry-Based Imperfection Measurement Tools to Determine the Impact of Corner Radii Imperfection on Cold-Formed Steel Member Strength,” Proc. of the Annual Stability Conference, Structural Stability Research Counsile, Baltimore, Maryland, 2018.

[17] ABAQUS, ABAQUS standard version 6.14-4, Dassault Systems Simulia Corp.

[18] E. Hognestad, “A study of Combined Bending and Axial Load in Reinforced Concrete Members,” Bulletin Series No. 399, Engineering Experiment Station, Urbana, USA: University of Illinois, 1951.